Activated-Ion Electron Transfer Dissociation Improves the Ability of Electron Transfer Dissociation to Identify Peptides in a Complex Mixture

ARTICLE *in* ANALYTICAL CHEMISTRY · NOVEMBER 2010

Impact Factor: 5.64 · DOI: 10.1021/ac1020358 · Source: PubMed

8 AUTHORS, INCLUDING:

Jae C Schwartz
Thermo Fisher Scientific
56 PUBLICATIONS **3,120** CITATIONS
SEE PROFILE

Jens Griep-Raming
Thermo Fisher Scientific
29 PUBLICATIONS **1,070** CITATIONS
SEE PROFILE

Published in final edited form as:
Anal Chem. 2010 December 15; 82(24): 10068–10074. doi:10.1021/ac1020358.

Activated-Ion ETD (AI-ETD) Improves the Ability of ETD to Identify Peptides in a Complex Mixture

Aaron R. Ledvina[1], **Nicole A. Beauchene**[1], **Graeme C. McAlister**[1], **John E. P. Syka**[3], **Jae C. Schwartz**[3], **Jens Griep-Raming**[4], **Michael S. Westphall**[1], and **Joshua J. Coon**[1,2,*]

[1] Department of Chemistry, University of Wisconsin, Madison, Wisconsin 53706

[2] Department of Biomolecular Chemistry, University of Wisconsin, Madison, Wisconsin 53706

[3] Thermo Fisher Scientific, San Jose, CA

[4] Thermo Fisher Scientific, Bremen, Germany

Abstract

Using a modified ETD-enabled QLT mass spectrometer, we demonstrate the utility of IR activation concomitant with ETD ion-ion reactions (activated-ion ETD, AI-ETD). Analyzing 12 SCX fractions of a LysC digest of human cells (HS) using ETD, CAD, and AI-ETD, we find that AI-ETD generates 13,405 peptide spectral matches (PSMs) at a 1% false-discovery rate (1% FDR), surpassing both ETD (7,968) and CAD (10,904). We also analyze 12 SCX fractions of a tryptic HS digest and find that ETD produces 6,234 PSMs, AI-ETD 9,130 PSMs, and CAD 15,209 PSMs. Compared to ETcaD, AI-ETD generates ~80% more PSMs for tryptic whole cell lysate and ~50% more PSMs for LysC whole cell lysate.

Introduction

Effective peptide fragmentation is a central component of shotgun proteomics, and the success of an experiment often depends upon the choice of fragmentation technique.[1–6] The ideal fragmentation method routinely produces a homologous series of product ions, allowing for confident identification of the interrogated peptide. The most common fragmentation techniques are based on activating a peptide *via* collisions with inert gas; such techniques comprise both ‘beam-type’ and resonant-excitation collision-activated dissociation (CAD).[7–10] Discovery-driven proteomics commonly utilizes CAD due to the high efficiency of fragmentation. During CAD, the selected precursor gains internal energy through collisions with neutral gas molecules until the energetic threshold of dissociation is reached. Though effective for peptide cations having a random series of protonated amide linkages, CAD’s success depends heavily on peptide charge and amino acid composition.[11, 12] Moreover, the presence of labile chemical moieties (*e.g.*, phosphoryl groups) leads to non-random fragmentation, as cleavage of the moiety often represents the lowest energy pathway. Consequent neutral loss of the labile group is thus the dominant CAD fragmentation pathway.[13, 14] While this issue has been somewhat mitigated via the use of an additional stage of fragmentation, limitations persist.[15] In addition to the duty cycle concerns associated with MS^3 neutral loss scanning for shotgun proteomics experiments, there have been at least two independent publications reporting that compared to CAD, MS^3 neutral loss scanning did not increase coverage of identified phosphopeptides and only slightly improved site localization.[16, 17] These limitations have sparked interest in the development of alternative peptide fragmentation methods.

*To whom correspondence should be addressed. jcoon@chem.wisc.edu.

Electron-based fragmentation strategies, *i.e.*, electron transfer dissociation (ETD) and electron capture dissociation (ECD), are attractive alternatives.[18–20] While generally less efficient than CAD (precursor-to-product conversion), these techniques demonstrate markedly lower dependence on peptide amino acid composition.[21, 22] A limitation of these techniques, however, is an increasing proclivity for non-dissociative electron transfer (ECnoD/ETnoD) with increasing precursor *m/z*.[22, 23] Practitioners of ECD utilize either pre- or concomitant peptide activation strategies (activated-ion ECD, AI-ECD) to mitigate the degree of ECnoD.[24–30] These strategies deposit internal vibrational energy through various means (*e.g.*, IR photons and collisions with gas), disrupting gas phase secondary structures and leading to more efficient ECD. ETD is conducted at pressures several orders of magnitude higher than those used in ECD; thus, peptide cations undergoing ETD are cooler, and pre-activation using either collisions or photons produces only transient (~1 ms) unfolding. A supplemental collisional activation step following the ETD ion-ion reaction, so-called ETcaD, is widely employed to circumvent ETnoD.[23, 31] With careful control of the activation conditions (*i.e.*, resonant activation *q*-value and amplitude), ETnoD species are converted almost exclusively into *c*- and *z*-type product ions. Though efficient for increasing peptide sequence coverage, ETcaD results primarily in the formation of odd electron $c^{\cdot}$- and even electron *z*-type ions, shifted ~ 1 Da from their theoretically predicted values. Consequently, ETcaD produces isotopic envelopes comprising a mixture of odd and even electron product ions, complicating spectral interpretation.[23]

Recently, we described the concomitant activation of peptide cations during ETD using IR photons, a process we term activated-ion ETD (AI-ETD).[32] AI-ETD successfully increases the sequence coverage of peptides beyond that attained using unassisted ETD, particularly for high *m/z* peptides. Moreover, AI-ETD results almost exclusively in production of odd electron $z^{\cdot}$-type and even electron *c*-type product ions, which match their theoretically predicted *m/z* values. As a proof of concept, our previous study considered only a handful of peptides and was not suitable for LC separations, an essential component of large-scale experiments. Here we present the modification of a quadrupole linear ion trap (QLT) mass spectrometer that allows AI-ETD to be conducted in an LC-compatible manner. Further, we use this platform to demonstrate the viability of AI-ETD as a peptide fragmentation method for large-scale protein sequence analysis.

Experimental Section

Cell Culture, Protein Harvest, and Protein Lysis

Human embryonic kidney (HEK) 293T cells were cultured to 90% confluency on 10cm plates containing high glucose (4.5g/L) dulbecco's modified eagle medium (DMEM) (GIBCO) with 1% fetal bovine serum (FBS) (GIBCO). Cell pellets were collected after two washes in dulbecco phosphate-buffered saline (DPBS) (GIBCO) and stored at −80°C. Upon lysis, the cell pellet was thawed and resuspended in 3mL of lysis buffer containing 8M urea, 75mM NaCl, 50mM Tris (pH 9), 50mM NaF, 1mM sodium orthovanadate, 6mM sodium pyrophosphate, complete mini EDTA-free protease inhibitor (Roche Diagonistics), and phosSTOP phophatase inhibitor (Roche Diagonotics). Lysis was accomplished via sonication. A 15 min room temperature spin at 3750 rpm allowed for collection of the supernatant.

Digestion

Approximately 3mL of lysis supernatant was subjected to 2.5mM DTT for 45 min at 37°C, followed by 7mM iodoacetamide for 30 min at room temperature to reduce and alkylate cysteine residues. Finally, an additional 2.5 mM DTT was added to the total volume for 15 min at room temperature. Two separate 500μg aliquots were isolated for subsequent

digestion by sequencing grade modified trypsin (Promega) and lysyl endopeptidase LysC (Wako Chemicals). The first aliquot was diluted to 1.5M urea, 50mM Tris, and 10mM $CaCl_2$ and digested with 5 μg of trypsin overnight at 37°C. The second aliquot was diluted to 2M urea, 25mM Tris, and 1mM $CaCl_2$ and digested with 5μg of LysC overnight at 37°C. The following morning, digestion reactions were quenched via addition of TFA to 0.5%. Each sample was desalted on a 50mg C_{18} SepPak cartridge (Waters). The individual eluates underwent lyophilization followed by storage at −20°C. For experimental use, eluates were resuspended in H_2O. SCX fractions of both trypsin- and LysC-digested whole cell lysates were prepared as previously described.[33]

Mass Spectrometry, LC separation

All experiments were performed on a modified LTQ-XL (Thermo Fisher Scientific, San Jose CA) linear ion trap mass spectrometer (QLT) utilizing a nanoESI source for the generation of precursor peptide cations and NCI source for the generation of reagent anions as previously described.[23] For all experiments, azulene was used as the ETD reagent ion. Instrument modifications are detailed below. All AI-ETD experiments were performed using a Firestar T-100 Synrad 120-W CO_2 continuous wave laser (Mukilteo, WA).

LC separations were carried out using a NanoAcquity UPLC system (Waters, Milford, MA) as previously described, using a 90 minute linear gradient from 1% to 35% acetonitrile followed by an additional 30 min at 1% acetonitrile for washing and equilibration for analysis of whole cell lysates and a similar 60 minute gradient for analysis of SCX fractions.[34, 35] For analysis of whole cell lysates, mass spectrometry methods consisted of an MS^1 scan followed by consecutive ETD, CAD, and AI-ETD data-dependent MS^2 scans of the two most intense precursors. For analysis of SCX fractions, an MS^1 scan was followed by MS^2 analysis of the six most intense precursors by ETD, CAD, or AI-ETD. Precursors were dynamically excluded for 90 s using an exclusion window of +/− 1.5 Th. AGC target values were 40 000 for MS^1 and 10 000 for MS^2 analysis. A representative LC-MS/MS analysis (both the raw data and search results) of LysC-digested sample has been uploaded and is available for public viewing (http://chem.wisc.edu/~coon/AI-ETD/).

Database Searching and Data Analysis

Data reduction was performed with DTA Generator as described previously.[22] OMSSA (version 2.1.7) was used to search spectra against the International Protein Index (IPI; http://www.ebi.ac.uk/IPI/) human database version 3.53.[36] Average mass tolerances of +/− 5 Th and +/− 0.5 Th were used for precursor and product *m/z*, respectively, with carbaminomethylation of cysteine set as a fixed modification and oxidation of methionine set as a variable modification. False discovery rates (FDR) were determined using the concatenated forward-reverse database searching method.[37, 38]

Results Section

Modification of QLT

In our initial description of AI-ETD, we modified a linear ion trap system to implement dual front-end ionization sources (APCI and ESI), which were pulsed for sequential generation of analyte cations and reagent anions.[32] This configuration provided a line of sight for delivery of photons concentric with the trapping volume at the far end of the linear ion trap. While effective for a preliminary evaluation, that arrangement was not suitable for large-scale LC-MS/MS analyses due to the lengthy duty cycle and ESI spray instabilities associated with pulsed spray voltages. We developed a new configuration in pursuance of our key goal for the present study: to evaluate AI-ETD for LC-MS/MS. The standard ETD-enabled linear ion trap utilizes a chemical ionization source for rapid, robust anion generation. This source

opposes the AP inlet as shown in Figure 1. Here we modified an instrument in this configuration by inserting a ZnSe window on the rear of the ETD module to transmit IR photons through a stainless steel aperture (diameter = 0.065″) concentric with the trapping volume of the QLT. To allow passage of IR photons to the trapping volume, the ion volume of the NCI source was modified by the addition of a hole (diameter = 0.070″) in the section of the ion volume farthest from the ion trap and the enlargement of the hole in the section closest to the ion trap, both concentric with the QLT trapping volume. We experimented with various diameters for the stainless steel disk, ranging from 0.020″ – 0.100″. For very small diameters, IR activation was inadequate for AI-ETD; conversely, for larger diameters, due to the laser beam impinging on the NCI source block and optics, the NCI source temperature increased substantially leading to decreased flux of reagent anions. The selection of 0.065″ represents a compromise, with effective IR activation and only minimal NCI source heating. Using this diameter disk, and 60W AI-ETD laser power over a 90 minute LC-MS/MS analysis, source temperature increased only marginally (~ 2° C).

Parametric evaluation of AI-ETD

Our initial studies indicated that laser power influences a number of factors, including the degree of hydrogen abstraction and intensity of product ions.[32] To characterize the effect of laser power on PSM generation for AI-ETD, we designed a series of experiments using AI-ETD at a range of laser powers (12, 24, 36, 48, and 60W) and utilizing a whole cell lysate previously digested with either trypsin or LysC. LC-MS/MS analyses were performed using consecutive ETD, CAD, and AI-ETD interrogation of the two most intense precursors from the MS^1 scan. At (AI-ETD) laser powers greater than 60 W, *b*- and *y*-type product ions resulting from precursor photo-dissociation are observed (data not shown).

In general, as laser power was increased, the degree of hydrogen abstraction we observed decreased; in practice this results in higher laser powers producing a greater proportion of odd electron *z*-type ions ($z^{\cdot}$-), and even electron *c*-type product ions (*c*-) than lower laser powers. To quantify the effect of such hydrogen abstractions, and also the overall product ion abundances, we considered AI-ETD performance as a function of laser power used (Table 1). PSM counts for both mixtures increase as laser power is increased from 12 to 48 W, followed by a mild decrease as power is increased to 60W. Next, PSMs binned by precursor *m/z* (50 Th wide) were plotted for the 12, 36, and 60 W experiments, normalized to the most PSMs for each individual bin (Figure 2). The use of 12 W generates the most PSMs for low m/z precursors (*m/z* = 300–400), with the most PSMs of moderate *m/z* precursors (*m/z* = 400–650) occurring using 36 W, and 60 W producing the most PSMs for high *m/z* peptides (*m/z* > 650).

To investigate this trend, we wrote software to search MS/MS spectra, of all PSMs (1% FDR) *en masse*, for the presence of *c*- and $z^{\cdot}$-type product ions. A product ion was considered present if the ion had S/N > 3 and the observed *m/z* value was within 0.25 Th of the theoretical value. We plotted the probability of observing the c_n- and z_n-type product ions as a function of *n* for ETD and AI-ETD at laser powers 12–60 W for all PSMs from the LysC dataset (Figure 3). For smaller ions ($c_1/z_1 - c_2/z_2$), as laser power increases, the probability of observation decreases; intermediate laser powers produce the highest probability of observation for moderate sized product ions ($c_3/z_3 - c_6/z_6$); larger product ions ($> c_6/z_6$) are most effectively generated using the highest laser powers.

A recent study by Han *et al.* found that collisional activation of ETD product ions results mostly in a-, b-, y-, and x- type product ions.[39] We anticipate IR activation of ETD product ions would have a similar effect. Thus secondary IR activation can decrease the probability of observing of *c*- and *z*-type product ions, particularly for smaller product ions because 1) they have fewer degrees of molecular freedom, meaning there will be fewer channels to

redistribute vibrational energy gained via infrared photons, and 2) they have lower *m/z* values, in consequence the reduced Mathieu parameter (*q*-value) will be higher during the activation process. Glish, Brodbelt, and others have noted that the *q*-value influences ion position within an ion trap. Higher *q*-values can result in deeper pseudo-potential wells, causing ions to spend a greater proportion of time in the center of the trap, and leading to a better overlap with the photon beam.[40, 41]

Larger fragment ions have a higher probability of being formed at more intense laser powers because they come from large peptides (*i.e.*, c_{12} is only formed by peptides of at least 13 residues), which have greater magnitudes of gas phase secondary structure. Higher laser powers most effectively disrupt this secondary structure, enhancing the probability of their formation. For moderate-sized ions, intermediate powers achieve the highest probability of formation; though sufficient to disrupt peptide secondary structure, this level of heating does not induce extensive secondary IR activation.

The probabilities of *c*- and $z^{\cdot}$- type product ion formation are the primary factor determining PSM numbers at different AI-ETD laser powers. The small product ions with less chance of being observed using AI-ETD conducted at high laser powers represent a relatively large percentage of all possible product ions for smaller precursors (*m/z* = 300–400), decreasing the probability of a PSM. Conversely, for peptide precursors with a high *m/z* value, the increased probability of observing the larger product ions more than compensates for the decreased probability of observing the first few ions, increasing the chance of a PSM. Because of this variability, we conclude that the most effective implementation of AI-ETD for shotgun proteomics is to set the laser power in a data-dependent manner, selecting modest laser powers for lower *m/z* peptide precursors and stronger laser powers for higher *m/z* peptide precursors.

Comparison of AI- ETD to ETD and CAD

The key motivation for this work was to evaluate the efficacy of AI-ETD as a fragmentation technique for interrogation of complex peptide mixtures as compared to current alternatives. Analyzing the data above and considering all three activation methods, AI-ETD (48 W) improves the numbers of PSMs relative to unassisted ETD for both tryptic and LysC analyses (Table 2). For LysC-digested peptides, the use of AI-ETD results in a substantial increase in PSMs relative to CAD; for trypsin-digested peptides, however, AI-ETD does not surpass CAD.

To determine which method is best for various types of peptide cations, we grouped the PSMs generated in these experiments based on precursor charge state (Table 3). The data contained within Table 3 demonstrate that for doubly protonated peptide precursors generated *via* either LysC or trypsin, CAD produces the most PSMs, although AI-ETD improves substantially upon ETD. For all other precursor charge states, for both tryptic and LysC peptides, AI-ETD identifies at least as many, and often more, peptides than either CAD or ETD.

SCX fraction analysis

Proteomic workflows often utilize two modes of separation prior to MS interrogation. To test the suitability of AI-ETD in this context, we next performed an experiment in which 12 SCX fractions of both LysC and tryptic digests were analyzed three times, using ETD, CAD, or AI-ETD. This experiment measures each activation technique based not only on the probability of PSM, but also on the duty cycle. AI-ETD laser power was set in a data-dependent manner, selecting laser power based upon precursor *m/z* and which power allowed for the highest probability of PSM for the whole cell lysate analyses (*vide supra*).

Briefly, for each LC-MS/MS experiment, AI-ETD PSMs were grouped by precursor *m/z* into bins 50 Th wide and divided by the number of ETD PSMs from the same analysis. Instrument firmware was then modified to automatically select the laser power yielding the most PSMs relative to ETD based upon precursor *m/z*. Analysis of the tryptic SCX fractions revealed that while use of AI-ETD resulted in 9,130 PSMs, a considerable improvement over unassisted ETD (6,234), CAD (15,209) produced the most PSMs (Table 4). However, for the LysC fractions, AI-ETD produced 13,405 PSMs, eclipsing both ETD (7,968) and CAD (10,904). Further, while CAD interrogation of tryptic SCX fractions produced the most PSMs, AI-ETD analysis of LysC SCX fractions produced the greatest proteome coverage, reflecting the larger average size of peptides generated by LysC.

Early eluting SCX fractions contain mostly peptides which ionize in low charge states (*i.e.*, +2); thus, CAD generates the most PSMs for these analyses, although AI-ETD produces more PSMs than ETD. The middle fractions contain peptides which tend to ionize in moderate charge states, such that ETD often outperforms CAD. However, AI-ETD greatly extends the *m/z* range for which peptides can be successfully interrogated relative to ETD, meaning that for the middle fractions AI-ETD frequently improves over both CAD and ETD. The later fractions contain mostly peptides which ionize in high charge states; thus, though both ETD and AI-ETD are well suited, AI-ETD consistently improves over ETD.

The key distinction between the two datasets is the types of peptides produced by each enzyme; trypsin generates peptides which mostly elute in the earlier fractions for which CAD is best suited. In consequence, CAD is the superior method overall for the tryptic SCX fractions, although AI-ETD offers the best option for the later fractions. LysC, on the other hand, produces peptides which more evenly distribute across all fractions. CAD still generates the most PSMs for the early fractions, but AI-ETD produces the most PSMs overall, since the middle and later fractions contain a larger proportion of all peptides.

AI-ETD vs. ETcaD

We next performed an experiment comparing AI-ETD (data-dependent laser power) with ETcaD using ES cell lysates generated via digestion with both trypsin and LysC (Table 5). AI-ETD results in improvement of ~50% (LysC) and ~80% (trypsin) in the number of PSMs generated over ETcaD. Because precursor charge state information is not available using a stand-alone ion trap, ETcaD was performed assuming a precursor charge state of +2, with the supplemental collisional activation step performed at an *m/z* value twice that of the precursor. An important comparison to make between AI-ETD and ETcaD, therefore, involves PSM numbers for doubly protonated peptides. By this metric, AI-ETD even more significantly improves over ETcaD, generating 2.4 (LysC) and 4.2 (Trypsin) times as many PSMs. We rationalize this improvement based on our previous observation that AI-ETD suffers less hydrogen abstraction than ETcaD; such abstractions produce even-electron *z*-type and odd-electron $c^{\cdot}$-type product ions, shifted by ~ 1 Da from their theoretically predicted value.[23]

Shown in Figure 4 are the AI-ETD and ETcaD scans of the doubly protonated precursor peptide ISSLLEEQFQQGK (*m/z* = 753). ETcaD and AI-ETD produce similar neutral loss patterns; this is expected as IRMPD and CAD are both considered ‘slow-heating’ dissociation methods.[6] Secondary IR activation of the charge-reduced precursor would thus produce similar results as the CAD activation step of ETcaD. While both ETcaD and AI-ETD also produce similar peptide sequence coverage, there is a marked difference between the types of product ions produced. AI-ETD produces nine *z*-type ions, eight of them odd electron ($z^{\cdot}$) and four *c*-type ions, all of them even electron. This near-complete sequence coverage and almost exclusive production of ions whose *m/z* values match those theoretically predicted yields a confident PSM (OMSSA evalue = 9.3×10^{-4}). In contrast,

ETcaD also produces nine *z*-type ions, only five of which are odd electron ($z^{\cdot}$), and 4 *c*-type ions, only one of which are even electron, respectively. These shifted product ions result in a dubious PSM (OMSSA e-value of = 1.8), insufficient to identify the peptide within 1% FDR range. Different spectral search algorithms may lead to slightly different results when comparing AI-ETD and ETcaD; however, we conclude superior spectral specificity makes concomitant supplemental activation techniques such as AI-ETD superior to post ion-ion reaction techniques like ETcaD.

AI-ETD for phosphopeptides

Because ETD is particularly well suited for the analysis of phosphopeptides, any method designed to augment ETD should be evaluated in this context.[42, 43] It is unclear whether the positive effects of AI-ETD will extend to phosphopeptides; Muddiman and others have noted that IRMPD of phosphopeptides results primarily in the neutral loss of the phosphoryl group.[44] The ETD, CAD, and AI-ETD spectra for doubly protonated peptide cation LRISSADsEK, (Figure 5) however, reveal that AI-ETD greatly enhances the fragmentation of this peptide relative to ETD. ETD produces 22% peptide sequence coverage, insufficient to localize the serine phosphorylation; in contrast, AI-ETD results in 89% sequence coverage and readily localizes the phosphorylation site. Application of CAD to this precursor produces a spectrum dominated by the neutral loss of H_3PO_4; however, sufficient backbone fragmentation is produced to generate 89% sequence coverage. This result, representing only a cursory evaluation, suggests that the efficacy of AI-ETD in the context of a large-scale study of phosphopeptides is worth evaluating. We note more comprehensive studies of AI-ETD for phosphopeptides are ongoing.

Conclusion

We have modified the hardware and firmware of an ETD-enabled QLT mass spectrometer, allowing for AI-ETD with upstream LC separations. Conducting a large-scale study, we conclude that for doubly protonated peptides, CAD is the most suitable activation method, although AI-ETD improves considerably over ETD. For all other peptide charge states, however, AI-ETD produces more PSMs (1% FDR) than both CAD and ETD. We evaluated the suitability of AI-ETD for large scale proteomics experiments by analyzing 12 SCX fractions generated with LysC and trypsin with ETD, CAD, and AI-ETD. For LysC, AI-ETD (13,405 PSMs), surpassed ETD (7,968) and CAD (10,904). Analysis of the tryptic SCX fractions reveals that while AI-ETD (9,130) improves upon the number of PSMs ETD produces (6,234), CAD generates the most PSMs (15,209) because more peptides are present in the earlier SCX fractions for which CAD is most effective.

We have demonstrated that the potential illustrated in our original description of AI-ETD (increased ETD fragmentation efficiency, little hydrogen abstraction) translates into a considerable boost in PSM numbers (1% FDR). Comparing AI-ETD to the previous ETD supplemental activation of choice, ETcaD, AI-ETD produces 80% (trypsin) and 50% (LysC) more PSMs. Improvements in AI-ETD duty cycle and implementation on hybrid MS platforms capable of providing precursor charge state information will improve AI-ETD further still. Moreover, real-time selection of the activation technique between CAD and AI-ETD based upon precursor *m/z* and charge state could potentially allow for the greatest probability of PSM. We conclude that such incorporation with CAD in a decision tree fashion will result in substantial improvements over either method individually, and would represent one of the most powerful peptide sequencing platforms described to date.

Acknowledgments

This work was supported by Thermo Fisher Scientific and the National Institutes of Health (NIH) grants R01 GM080148 and P01 GM081629.

References

1. Hunt DF, Yates JR, Shabanowitz J, Winston S, Hauer CR. Proceedings of the National Academy of Sciences of the United States of America. 1986; 83:6233–6237. [PubMed: 3462691]
2. Aebersold R, Mann M. Nature. 2003; 422:198–207. [PubMed: 12634793]
3. Coon JJ, Syka JEP, Shabanowitz J, Hunt DF. Biotechniques. 2005; 38:519. [PubMed: 15884666]
4. de Godoy LMF, Olsen JV, Cox J, Nielsen ML, Hubner NC, Frohlich F, Walther TC, Mann M. Nature. 2008; 455:1251–U1260. [PubMed: 18820680]
5. Washburn MP, Wolters D, Yates JR. Nature Biotechnology. 2001; 19:242–247.
6. Sleno L, Volmer DA. Journal of Mass Spectrometry. 2004; 39:1091–1112. [PubMed: 15481084]
7. Hunt DF, Buko AM, Ballard JM, Shabanowitz J, Giordani AB. Biomedical Mass Spectrometry. 1981; 8:397–408. [PubMed: 7306675]
8. Mcluckey SA. Journal of the American Society for Mass Spectrometry. 1992; 3:599–614.
9. Verentchikov AN, Ens W, Standing KG. Analytical Chemistry. 1994; 66:126–133. [PubMed: 8116874]
10. Morris HR, Paxton T, Dell A, Langhorne J, Berg M, Bordoli RS, Hoyes J, Bateman RH. Rapid Communications in Mass Spectrometry. 1996; 10:889–896. [PubMed: 8777321]
11. Wysocki VH, Tsaprailis G, Smith LL, Breci LA. Journal of Mass Spectrometry. 2000; 35:1399–1406. [PubMed: 11180630]
12. Dongre AR, Jones JL, Somogyi A, Wysocki VH. Journal of the American Chemical Society. 1996; 118:8365–8374.
13. Schroeder MJ, Shabanowitz J, Schwartz JC, Hunt DF, Coon JJ. Analytical Chemistry. 2004; 76:3590–3598. [PubMed: 15228329]
14. DeGnore JP, Qin J. Journal of the American Society for Mass Spectrometry. 1998; 9:1175–1188. [PubMed: 9794085]
15. Olsen JV, Mann M. Proceedings of the National Academy of Sciences of the United States of America. 2004; 101:13417–13422. [PubMed: 15347803]
16. Ulintz PJ, Yocum AK, Bodenmiller B, Aebersold R, Andrews PC, Nesvizhskii AI. Journal of Proteome Research. 2009; 8:887–899. [PubMed: 19072539]
17. Villen J, Beausoleil SA, Gygi SP. Proteomics. 2008; 8:4444–4452. [PubMed: 18972524]
18. Zubarev RA, Kelleher NL, McLafferty FW. Journal of the American Chemical Society. 1998; 120:3265–3266.
19. Syka JEP, Coon JJ, Schroeder MJ, Shabanowitz J, Hunt DF. Proceedings of the National Academy of Sciences of the United States of America. 2004; 101:9528–9533. [PubMed: 15210983]
20. Coon JJ, Syka JEP, Schwartz JC, Shabanowitz J, Hunt DF. International Journal of Mass Spectrometry. 2004; 236:33–42.
21. Good DM, Coon JJ. Biotechniques. 2006; 40:783–789. [PubMed: 16774122]
22. Good DM, Wirtala M, McAlister GC, Coon JJ. Molecular & Cellular Proteomics. 2007; 6:1942–1951. [PubMed: 17673454]
23. Swaney DL, McAlister GC, Wirtala M, Schwartz JC, Syka JEP, Coon JJ. Analytical Chemistry. 2007; 79:477–485. [PubMed: 17222010]
24. Oh HB, McLafferty FW. Bulletin of the Korean Chemical Society. 2006; 27:389–394.
25. Oh H, Breuker K, Sze SK, Ge Y, Carpenter BK, McLafferty FW. Proceedings of the National Academy of Sciences of the United States of America. 2002; 99:15863–15868. [PubMed: 12444260]
26. Breuker K, Oh HB, Horn DM, Cerda BA, McLafferty FW. Journal of the American Chemical Society. 2002; 124:6407–6420. [PubMed: 12033872]

27. Senko MW, Speir JP, Mclafferty FW. Analytical Chemistry. 1994; 66:2801–2808. [PubMed: 7978294]
28. Cooper HJ, Hakansson K, Marshall AG. Mass Spectrometry Reviews. 2005; 24:201–222. [PubMed: 15389856]
29. Horn DM, Ge Y, McLafferty FW. Analytical Chemistry. 2000; 72:4778–4784. [PubMed: 11055690]
30. Ben Hamidane H, Chiappe D, Hartmer R, Vorobyev A, Moniatte M, Tsybin YO. Journal of the American Society for Mass Spectrometry. 2009; 20:567–575. [PubMed: 19112028]
31. Xia Y, Han H, McLuckey SA. Analytical Chemistry. 2008; 80:1111–1117. [PubMed: 18198896]
32. Ledvina AR, McAlister GC, Gardner MW, Smith SI, Madsen JA, Schwartz JC, Stafford GC, Syka JEP, Brodbelt JS, Coon JJ. Angewandte Chemie-International Edition. 2009; 48:8526–8528.
33. Swaney DL, McAlister GC, Coon JJ. Nature Methods. 2008; 5:959–964. [PubMed: 18931669]
34. Zhang Y, Ficarro SB, Li SJ, Marto JA. Journal of the American Society for Mass Spectrometry. 2009; 20:1425–1434. [PubMed: 19403316]
35. McAlister GC, Phanstiel D, Wenger CD, Lee MV, Coon JJ. Analytical Chemistry. 2010; 82:316–322. [PubMed: 19938823]
36. Geer LY, Markey SP, Kowalak JA, Wagner L, Xu M, Maynard DM, Yang XY, Shi WY, Bryant SH. Journal of Proteome Research. 2004; 3:958–964. [PubMed: 15473683]
37. Moore RE, Young MK, Lee TD. Journal of the American Society for Mass Spectrometry. 2002; 13:378–386. [PubMed: 11951976]
38. Elias JE, Gygi SP. Nature Methods. 2007; 4:207–214. [PubMed: 17327847]
39. Han HL, Xia Y, McLuckey SA. Journal of Proteome Research. 2007; 6:3062–3069. [PubMed: 17608403]
40. Gardner MW, Smith SI, Ledvina AR, Madsen JA, Coon JJ, Schwartz JC, Stafford GC, Brodbelt JS. Analytical Chemistry. 2009; 81:8109–8118. [PubMed: 19739654]
41. Remes PM, Glish GL. Journal of Physical Chemistry A. 2009; 113:3447–3454.
42. Swaney DL, Wenger CD, Thomson JA, Coon JJ. Proceedings of the National Academy of Sciences of the United States of America. 2009; 106:995–1000. [PubMed: 19144917]
43. Grimsrud PA, Swaney DL, Wenger CD, Beauchene NA, Coon JJ. Acs Chemical Biology. 2010; 5:105–119. [PubMed: 20047291]
44. Flora JW, Muddiman DC. Analytical Chemistry. 2001; 73:3305–3311. [PubMed: 11476230]

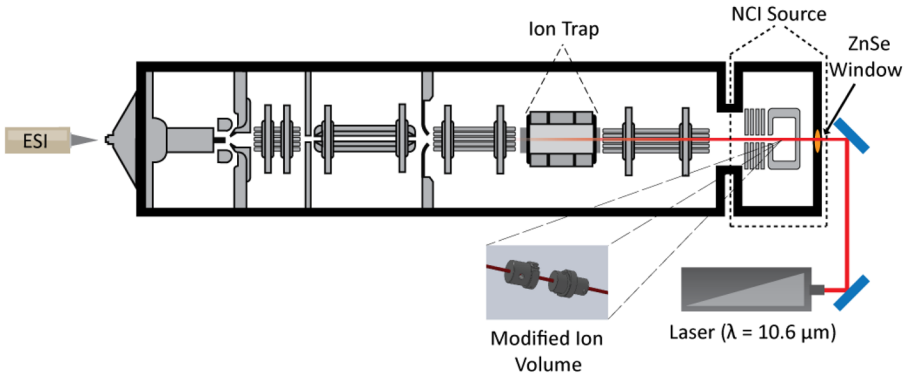

Figure 1.
Modified QLT allowing for IR activation concomitant to ETD ion-ion reactions.

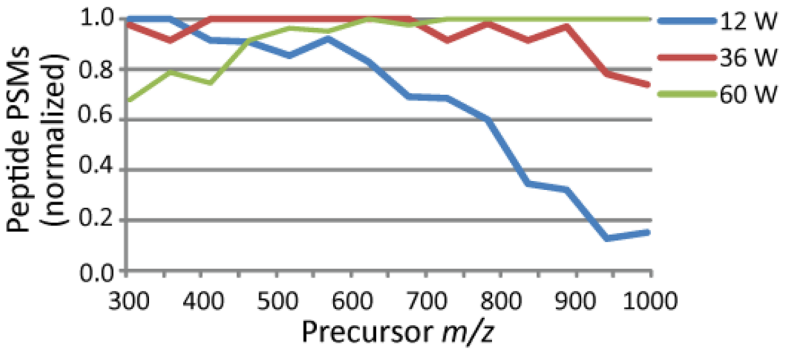

Figure 2.
Peptide Spectral Matches as a function of precursor peptide *m/z* for AI-ETD at 12, 36, and 60 W AI-ETD laser power.

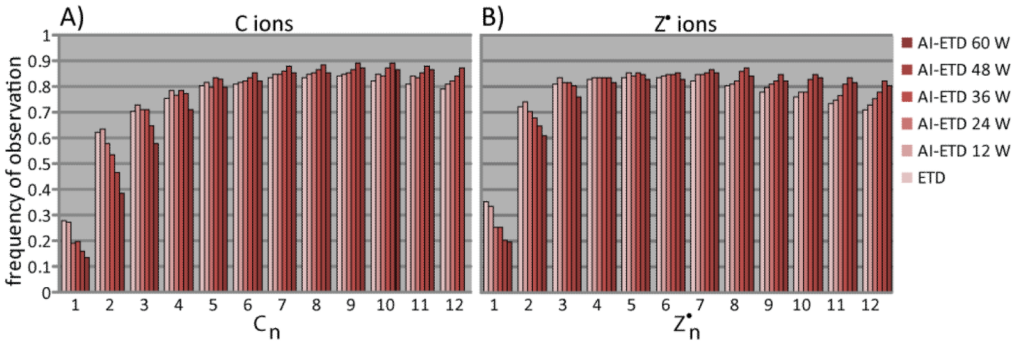

Figure 3.

The probability of observing c_n- (A) and z_n- (B) as a function of n for ETD and AI-ETD at various laser powers. At low *n* values, low laser powers result in the greatest chance of observation, but with increasing n, higher laser powers lead to the highest probability of observation.

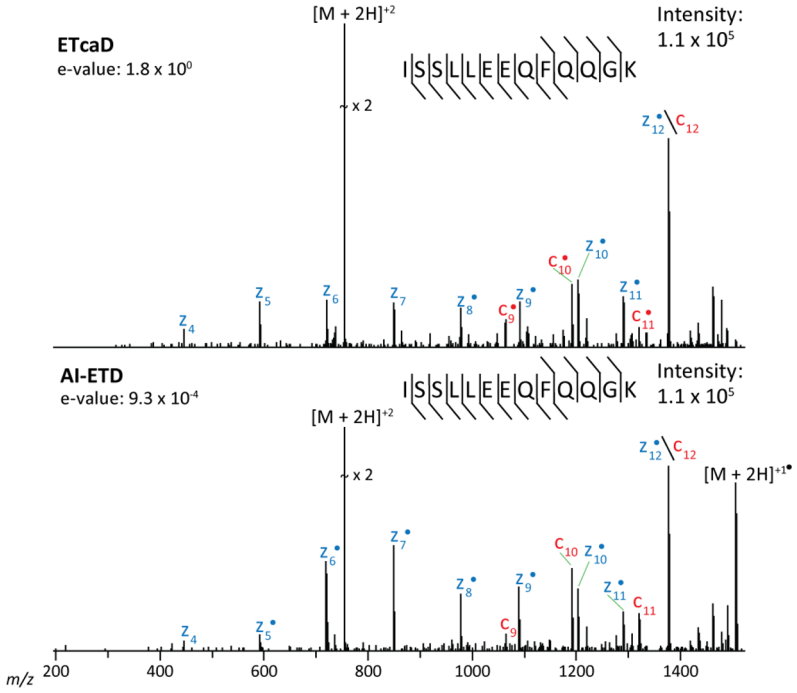

Figure 4.

Spectra (single scan) resulting from either ETD (A) or AI-ETD (B) following dissociation of the doubly protonated peptide cation ISSLLEEQFQQGK. AI-ETD results almost exclusively in the formation of *c*- and *z*˙- type ions which match their theoretically predicted *m/z* values.

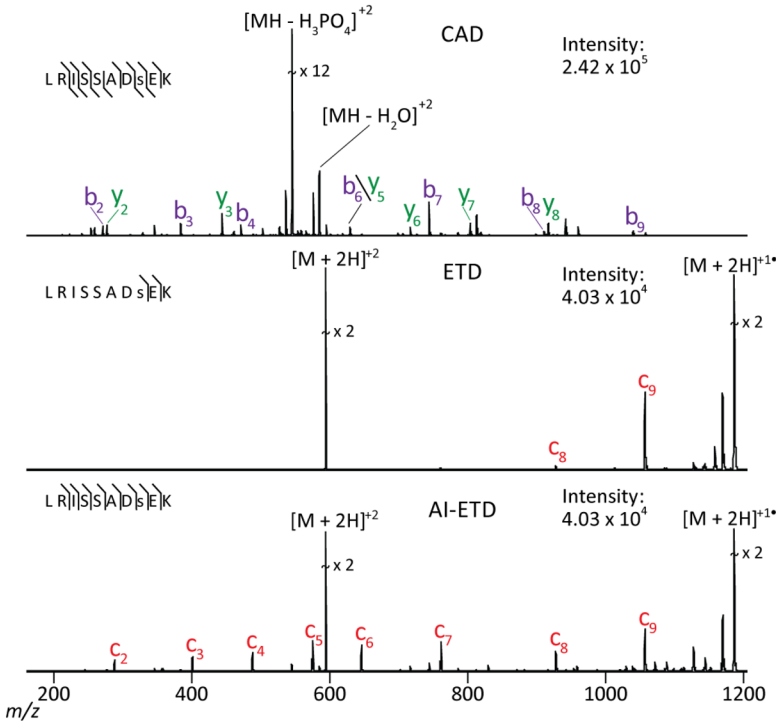

Figure 5.

Spectra (single scan) resulting from either ETD (A) or AI-ETD (B) of the doubly protonated phosphopeptide cation LRISSADsEK.

Table 1

AI-ETD peptide spectral matches at various laser powers

PSM numbers (1 % FDR) for AI -ETD at various laser powers.

	Lysine-C	Trypsin
AI-ETD (12 W)	1354	982
AI-ETD (24 W)	1566	1180
AI-ETD (36 W)	1841	1304
AI-ETD (48 W)	2022	1377
AI-ETD (60 W)	1980	1308

* denotes the average of 5 LC experiments

Table 2
AI-ETD, ETD, and CAD peptide spectral matches

PSMs for ETD, CAD, and AI-ETD for both LysC and Tryptic digests.

MS^2 Activation	Lysine-C	Trypsin
ETD*	1289	915
CAD*	1366	2167
AI-ETD	2022	1377

*denotes the average of 5 LC experiments

Table 3

AI-ETD, ETD, and CAD peptide spectral matches sorted by precursor charge state

PSMs for ETD, CAD, and AI-ETD for both LysC and tryptic digests grouped by precursor charge state.

MS^2 Activation	Lysine-C precursor charge state IDs				Trypsin precursor charge state IDs			
	+2	+3	+4	≥+5	+2	+3	+4	≥+5
ETD*	3	506	493	287	2	605	248	60
CAD*	360	624	287	95	1059	871	204	33
AI-ETD	73	819	677	453	140	860	299	78

*denotes the average of 5 LC experiments

Table 4

ETD, AI-ETD, and CAD PSMs

PSM numbers and proteome coverage resulting from analysis of 12 SCX fractions from both LysC and trypsin digest using ETD, CAD, and AI-ETD.

	LysC peptide Identifications			Trypsin peptide Identifications		
	ETD	**AI-ETD**	**CAD**	**ETD**	**AI-ETD**	**CAD**
Fraction 1–2	33	151	291	1	5	83
Fraction 3	247	444	1633	339	655	1544
Fraction 4	271	1050	2113	211	826	4443
Fraction 5	1073	1998	1789	763	1486	3044
Fraction 6	1454	1967	1400	1334	1535	2209
Fraction 7	1282	2354	1224	984	1323	1337
Fraction 8	870	1509	1035	935	1047	970
Fraction 9	776	1442	673	568	908	668
Fraction 10	386	563	200	621	789	609
Fraction 11	870	950	234	408	477	277
Fraction 12	706	977	312	70	79	25
Total Peptides	7,968	13,405	10,904	6,234	9,130	15,209
Total Amino Acid coverage	146,343	281,120	212,834	96,779	150,485	241,070

Table 5
AI-ETD and ETcaD, peptide spectral matches

Comparison of AI-ETD and ETcaD using both tryptic and LysC digested whole cell lysates indicates that AI-ETD is superior for peptide precursors of all charge states and doubly protonated precursors.

	AI-ETD	ETcaD
Lys C; all z	2978	1940
Lys C; z=2	199	58
Trypsin; all z	2441	1344
Trypsin; z=2	367	70